Boron-Mediated Nanotube Morphologies

Rebecca J. Nicholls,[†,*] Zabeada Aslam,[†] Michael C. Sarahan,[‡,§] Antal Koós,[†] Jonathan R. Yates,[†] Peter D. Nellist,[†] and Nicole Grobert[†]

[†]Department of Materials, University of Oxford, Parks Road, Oxford OX1 3PH, U.K. and [‡]SuperSTEM Laboratory, STFC Daresbury, Keckwick Lane, Warrington WA4 4AD, U.K. [§]Present address: Gatan, Inc., 5794 W. Las Positas Blvd., Pleasanton, CA 94588, United States.

ABSTRACT

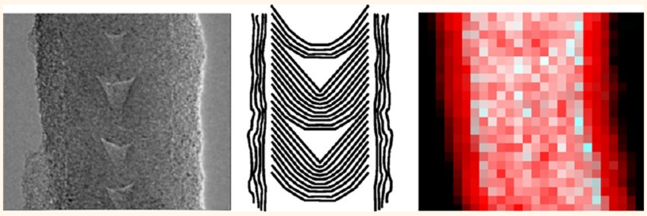

The “doping” of carbon nanotubes with heteroatoms is an established method of controlling their properties. However, variations in heteroatom concentration in multiwalled carbon nanotubes (MWCNTs) tend to produce nanotubes with different morphologies, and hence varying properties, within the same sample. Electron energy loss spectroscopy in conjunction with imaging using a scanning transmission electron microscope (STEM) is a powerful tool to precisely map the spatial variation and bonding state of heteroatoms, *e.g.*, B, N, P, Si, or combinations of these, present in carbon nanotubes exhibiting different structures. TEM analysis revealed that B incorporation during MWCNT growth (B-MWCNTs) results in nanotube morphologies that can be divided into three different types. These include core—shell structures possessing a B-rich core of cones and a C outer layer, B-containing cone structures, and MWCNTs with an irregular inner channel. *In situ* studies were carried out using Nanofactory holder experiments in order to investigate the properties of individual B-MWCNTs and to show that the three types of nanotubes undergo different current-induced breakdown. The inhomogeneity in composition, structure, and properties of B-MWCNTs could result from the variation in chemical composition and temperature within the furnace, and this work highlights the importance of developing synthesis techniques that can control the inclusion of heteroatoms into nanotubes.

KEYWORDS: boron multiwalled nanotubes · EELS · STEM

Boron can be incorporated into carbon nanotubes (CNTs) to control their chemical and physical properties.[1−4] Previous work by Carroll *et al.*[5] showed that there are variations in the local density of states along the length of B-containing arc-discharge multiwalled carbon nanotubes (B-MWCNTs$_{\mathrm{arc}}$), indicating that changes could occur in the chemical composition along the length of the nanotubes. Satishkumar *et al.*[6] found that the amount of B in B-MWCNTs$_{\mathrm{arc}}$ can vary from nanotube to nanotube, from about two to four atomic percent. Such variations in B concentration from nanotube to nanotube, or even across a single nanotube, are likely to lead to local changes in the chemical and physical properties. Broad beam methods or bulk methods can provide only average information about the composition of a material, but fail to provide local information. In order to understand how B is incorporated into nanotubes and to be able to control the properties of nanotubes, it is vital to map compositional and chemical changes across single nanotubes at the nanometer scale.

Scanning transmission electron microscopes (STEMs) equipped with spectrometers that allow electron energy loss spectroscopy (EELS) can combine high-spatial-resolution imaging and chemical analysis. EELS ionization edges resulting from the beam exciting core electrons within the sample can be used to identify the elements present in a nanotube. The fine structure of the edge can provide information about the bonding environment of the atom. By obtaining a spectrum image, *i.e.*, obtaining a spectrum at each illumination point while scanning the beam across a sample, elemental maps of a material can be produced that supply information about the chemical state of the elements at each point.

In this paper, we investigate the morphology and local chemical composition of B-MWCNTs produced using aerosol-assisted chemical vapor deposition techniques. Our studies reveal that there are three types of B-MWCNTs, each exhibiting a different morphology and a distinct chemical composition. The difference in morphology is most likely due to the fact that the B is not distributed uniformly across the sample and that only two of the three types of MWCNTs actually contain B. Since one of the main motivations behind the inclusion of heteroatoms is to alter the electronic properties of the nanotubes, *in situ*

* Address correspondence to rebecca.nicholls@materials.ox.ac.uk.

Received for review April 23, 2012 and accepted August 10, 2012.

10.1021/nn301770b

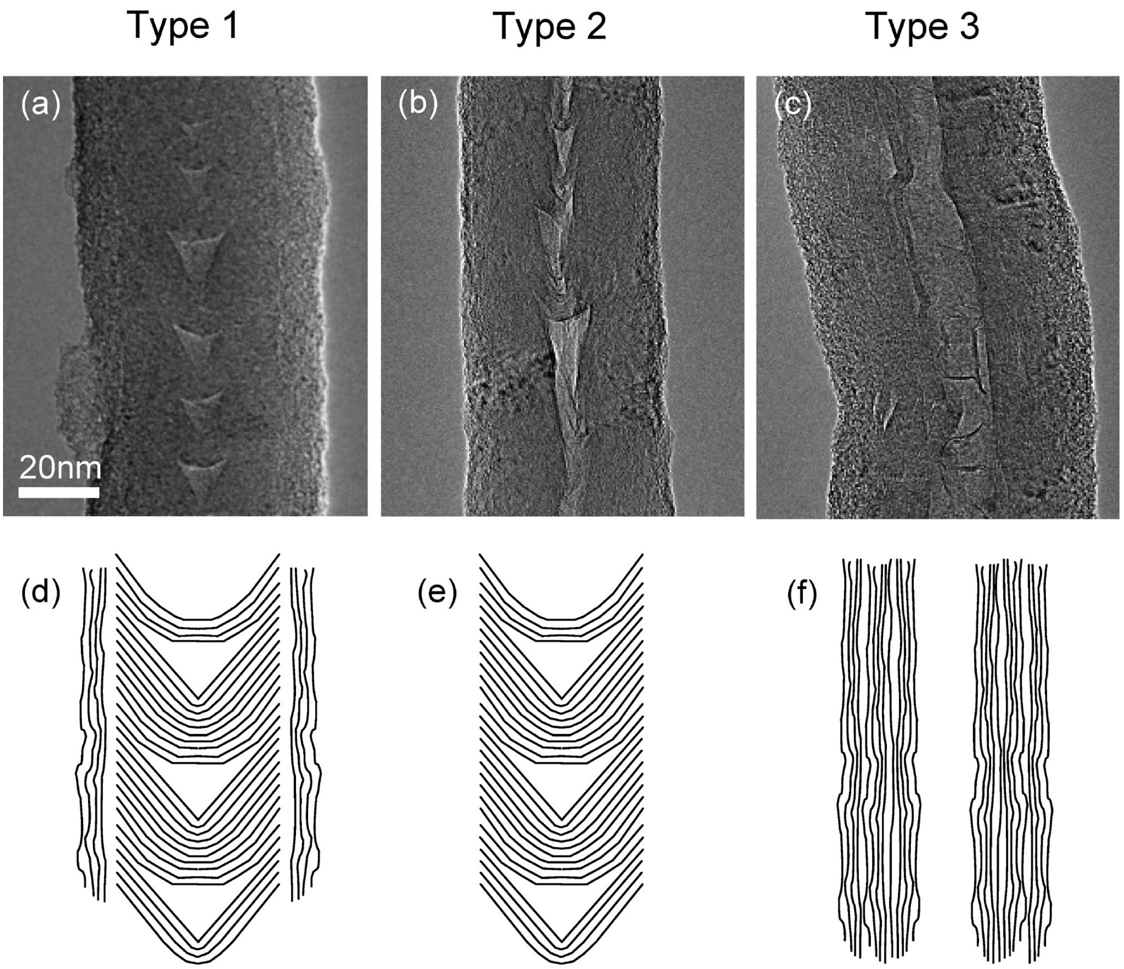

Figure 1. Three different types of B-MWCNT. (a−c) Bright field TEM images and (d−f) schematic representations of (a), (b), and (c), respectively.

experiments were carried out in order to observe the behavior of the three types of MWCNTs when current was passed through them, and as anticipated, the mechanism of current-induced breakdown was found to be different for each of the morphologies observed.

RESULTS AND DISCUSSION

Imaging of the B-MWCNT sample was carried out using a transmission electron microscope (TEM). Three different nanotube morphologies were observed within a B-MWCNT batch sample. An example of the first morphology (which will be referred to as type 1) is shown in Figure 1a. The nanotube exhibits a well-defined cone structure surrounded by a more disordered outer layer, as depicted schematically in Figure 1d. A nanotube with the second morphology (type 2) is shown in Figure 1b. Type 2 nanotubes have a well-defined cone structure, similar to type 1 nanotubes, but without the thick disordered outer layer (see Figure 1e), and, as we will see later, show a different chemical composition. The third morphology (type 3) does not exhibit a cone structure, and the inner channel of the type 3 nanotubes is irregular and varies in width along their length. The walls are more disordered than the cone structures, but not as much as the type 1 outer layer. An example of a type 3 nanotube is shown in Figure 1c with a schematic representation in Figure 1f.

EELS maps were obtained from each of the three morphologies in order to investigate their local chemistry. Figure 2 shows a high-angle annular dark field (HAADF) image and elemental map of a type 1 B-MWCNT. The B signal is associated with the cone-structured core of the nanotube, while the disordered outer layer consists of carbon only. A previous study of B-MWCNTs by Hsu *et al.*[7] found B frequently at the end of the nanotubes. The B-MWCNTs studied by Hsu *et al.* were prepared by arc-discharge methods, *i.e.*, at very high plasma temperatures, compared with chemical vapor deposition techniques operated at 800−1000 °C, which are used to produce the B-MWCNTs studied here. The nanotube tips examined by Hsu *et al.* showed cones, and that result is consistent with the findings here that show B is associated with the cone structures.

A typical EELS B K-edge obtained from the core of a type 1 nanotube is shown in Figure 3a. A K-edge is an excitation of a 1s core electron, and the fine structure within the edge results mainly from excitations to the

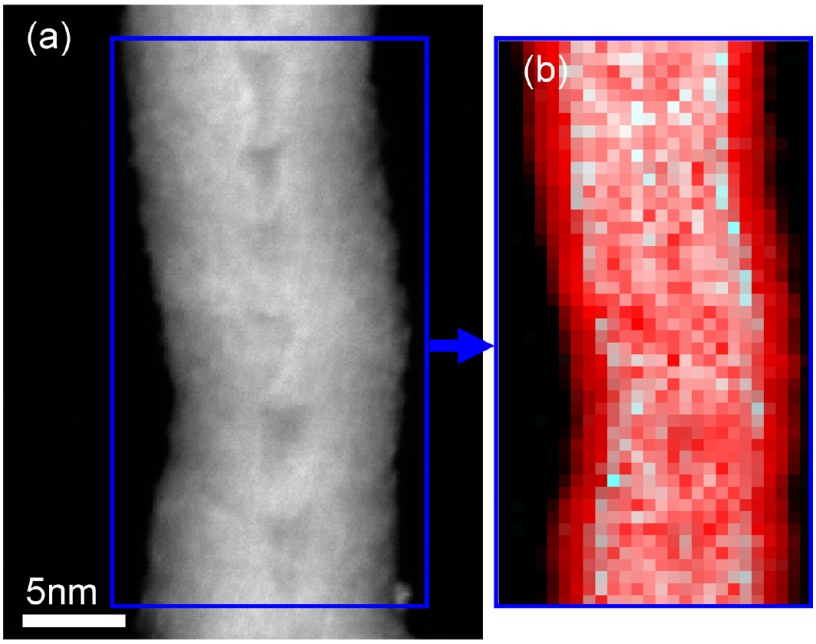

Figure 2. (a) HAADF image of a type 1 nanotube. (b) Elemental map of the area marked in (a) with C shown in red and B in cyan (the combination of red and cyan produce white), revealing a core–shell structure whereby B was found only in the central core of the type 1 B-MWCNT. The pixel size for (b) is 0.57 nm × 0.57 nm.

2p unoccupied states. If the 2p electrons are sp^2, or π bonded, a feature known as a π^* peak appears close to the edge onset in the EELS spectrum. The spectrum in Figure 3a does not exhibit a strong π^* feature and is similar to the spectrum from amorphous B.[8] B atoms situated substitutionally within flat graphene would be expected to produce a π^* feature,[9] and hence we conclude that the B within the cones is not bonded in this way. Figure 3b is a B spectrum obtained from the interface of the core and disordered outer region. In this case, there is a reproducible π^* peak (at 192 eV), indicating that some π bonding is present.

A HAADF image of a type 2 nanotube is shown in Figure 4a, along with a map of the B K-edge EELS signal (Figure 4b). The 2D spectrum image shows two different B K-edges. The first (Figure 3c) has no π^* peak and is similar in shape to the typical type 1 spectrum. The second (Figure 3d) has a sharp π^* peak, at 193.5 eV, which is shifted in energy compared to the π^* peak from the interface of the type 1 nanotube. The spectrum in Figure 3d also has a strong feature at 202.5 eV, and the fine structure of the spectrum is similar to that of B_2O_3, which has a π^* peak at 194.5 eV and a strong feature at 202.5 eV.[8] This match cannot be achieved with any other simple B compound, such as hexagonal BN. A map of the B π^* peak (Figure 4c) shows that the feature is mainly found toward the surface of the nanotube, and a corresponding oxygen map shows O is also present (the B π^* map is repeated in Figure 4d with the O map inserted on top). No O signal was detected in the type 1 nanotube. It is likely that the type 2 nanotube contains boron oxide, and the slight decrease in energy of the π^* peak compared with the boron oxide reference suggests that the bonding environment deviates from the typical B_2O_3. The boron oxides may form during the synthesis process as the nanotubes are grown on a SiO_2 substrate, which would provide a source of O. Alternatively, the lack of an outer C shell may mean that the B oxidizes on exposure to air after synthesis. EELS mapping of type 3 nanotubes generally did not show a B EELS signal, and so the type 3 nanotubes contained less than the detectable limit of B.

The diameter distribution for B-MWCNTs has been previously determined by Koós *et al.*[1] They found a broad distribution with peaks at 30 and 90 nm. The smaller diameter B-MWCNTs tend to tangle, making it difficult to get accurate statistics of the relative amount of each type of nanotube. By grouping 114 nanotubes according to type we found that the majority of the nanotubes (~87%) are type 3, and only a couple of percent are type 2. Most of the nanotubes with large diameters are type 3. The nanotubes with small diameters are a mixture of all three types, and the small-diameter type 3 nanotubes can be coiled with boron oxide nanoparticles on, or near, the surface.

The properties of materials are governed by their atomic structure. Therefore, the different morphologies and chemical composition of the three types of B-MWCNT are likely to result in different properties. By understanding under exactly what conditions each of the structures form, it may be possible to gain greater control of the morphologies produced and, therefore, the properties of the ensemble of the nanotubes, *i.e.*, the bulk sample.

Modification of electrical properties is one of the motivations for incorporating B into nanotubes.[4] It is therefore important to know how the different types of nanotube behave when current is passed to gauge the potential of the structures for electrical applications. Electrical transport measurements were carried out *in situ* in the TEM on all three types of nanotube in which the bias, and corresponding current, across the nanotube was increased until it broke down.

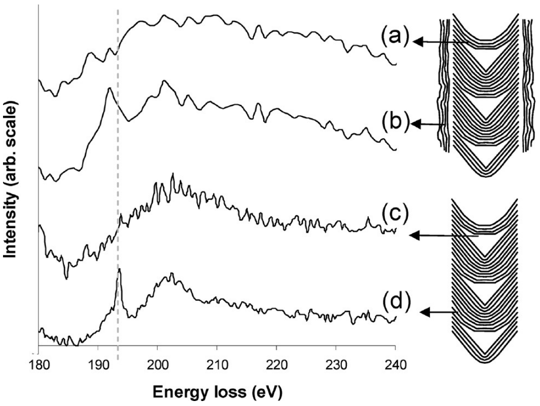

Figure 3. (a) Typical B K-edge from the core of a type 1 nanotube. (b) B K-edge from the interface between the core and the outer layer in a type 1 nanotube. (c) B K-edge from the center of a type 2 nanotube. (d) B K-edge from the edge of a type 2 nanotube.

Figure 5 shows a type 1 nanotube before current was applied (a), during current flow (b), and after the nanotube broke down (c). At the beginning of the experiment the nanotube has the expected core−shell structure, and as current is passed, the two regions become more defined and begin to separate with small voids forming. One such void is indicated by an arrow in Figure 5b. As shown earlier, the core and shell of the coaxial nanotube have different chemical compositions, and it is likely that they will have different thermal expansion properties. Expansion of the core and shell at different rates as a result of Joule heating

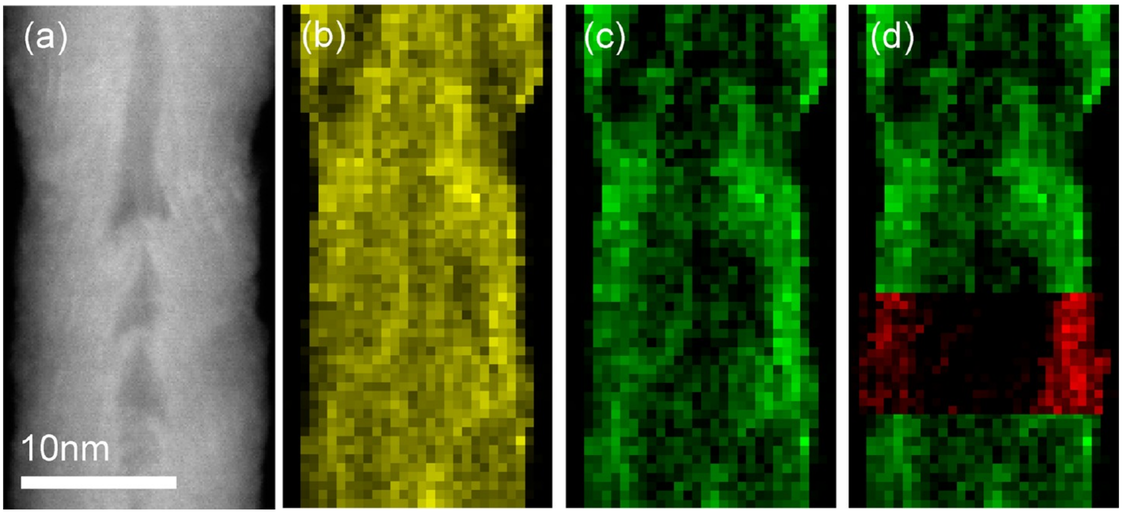

Figure 4. (a) HAADF image of a type 2 nanotube. (b) B elemental map (yellow). (c) Map of the B π^* peak (green). (d) Map of the B π^* peak (green) with O elemental map inserted (red). The pixel size for the B maps is 0.44 nm × 0.58 nm and for the O map is 0.51 nm × 0.51 nm.

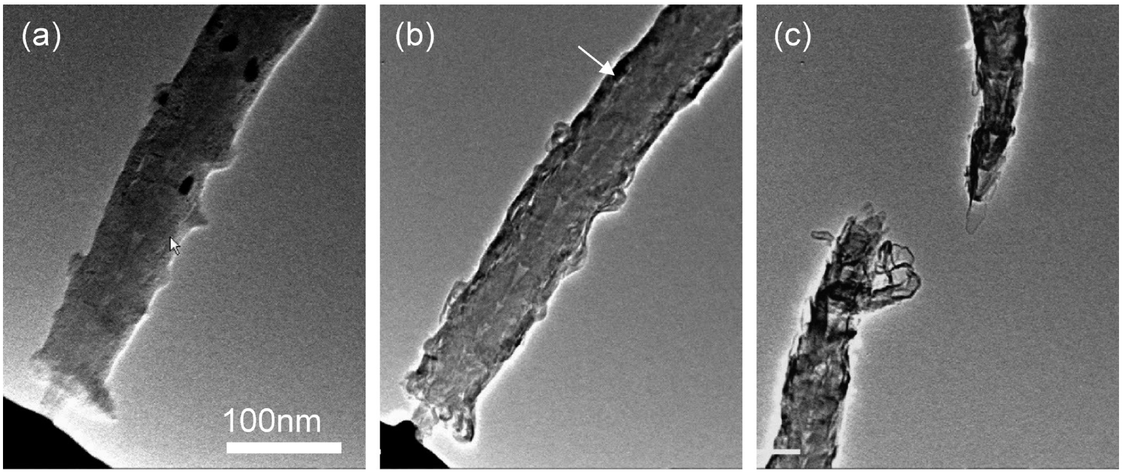

Figure 5. Type 1 B-MWCNT (a) before current flow, (b) during current flow, and (c) after breakdown.

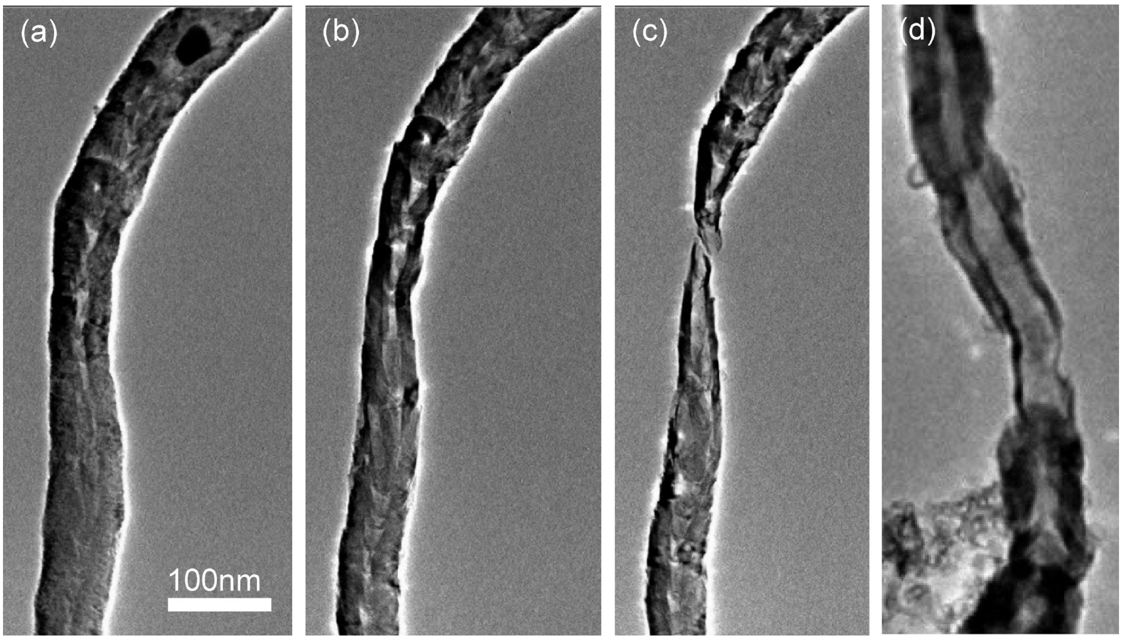

Figure 6. Type 2 B-MWCNT (a) before current flow, (b) during current flow, and (c) after breakdown. (d) Type 3 nanotube becoming thinner as the current flows.

caused by the current would explain the delamination of the two regions.[10] As the current continues to flow, the outer shell begins to disappear. The nanotube then breaks, leaving cones exposed. Previously we showed that the electronic behavior of this type of nanotube changes from metallic to semiconducting as the outer shell is removed.[10] For the nanotube shown in Figure 5, the breakdown current was 187 μA, which corresponds to a maximum current density of 4.9 × 10^6 A cm^{-2}. From the $I-V$ curve, the value of resistivity for this nanotube was found to be 3.4 × 10^{-5} Ωm. This value is higher than the value of resistivity perpendicular to the *c*-axis for graphite (9.8 × 10^{-6} Ωm[11]), but smaller than the resistivity parallel to the *c*-axis (4.1 × 10^{-5} Ωm[11]). This is in keeping with the combination of cones and the disordered outer layers. The cones are formed from defect-containing graphitic planes that are neither parallel nor perpendicular to the *c*-axis. The outer layers are defective, and the so the resistivity would be expected to be higher than that for the value of graphite perpendicular to the *c*-axis.

Figure 6a–c show the effect of current on a type 2 nanotube. In this case there is no outer shell and no separation takes place. As the current flows, the cone structure becomes more defined and the nanotube breaks in a similar way to the type 1 nanotube, leaving cones exposed. For this nanotube, the breakdown current was 253 μA, corresponding to a maximum current density of 5.8 × 10^6 A cm^{-2}. The resistivity of this nanotube, measured from $I-V$ curves, was found to be 7.8 × 10^{-5} Ωm, which is higher than both the value for the type 1 nanotube (Figure 5) and measurements conducted parallel to the *c*-axis in graphite. The higher resistivity could be due to the defects necessary to form the cone and the presence of the boron oxide as well as the lack of an outer carbon layer. Figure 6d shows the effect of current on a type 3 nanotube that has no cones; it becomes thinner until it eventually breaks.

CONCLUSION

Uniform doping or controlled modification of MWCNTs with heteroatoms is not a simple task. Our findings revealed that heteroatom-containing MWCNT samples consist of an ensemble of nanostructures. In our particular case, we showed that an ensemble of B-MWNTs contained at least three distinct types of nanostructure, whereby the first morphology (type 1) is a core–shell structure consisting of a B-rich cone-structured core and a disordered carbon outer layer. The EELS fine structure indicated that the B was not incorporated substitutionally into the core of the type 1 nanotube, but that there was some π bonding at the interface between the core and outer shell. The second structure (type 2) is similar to type 1 but without the disordered carbon shell, and boron oxide is found toward the surface of the type 2 nanotubes instead. In contrast to type 1 and type 2 nanotubes, the third type of nanotube (type 3) exhibited an inner channel of variable width, and neither possessed cones nor was any B detected. Furthermore, using *in situ* current experiments we showed that, as a result of these structural and chemical variations within the ensemble, the three different types of nanotubes follow different current-induced breakdown mechanisms, suggesting that variations in local chemistry within the ensemble indeed results in local property variations. Our findings, therefore, highlight the importance of using local characterization techniques for a better understanding of nanomaterials, such as doped CNTs, and their suitability as either individual structures or ensembles as components for future technological applications.

MATERIALS AND METHODS

B-MWCNTs were synthesized using an aerosol-based CVD system from a 9:1 mixture of toluene and 1 M triethylborane solution in hexane at 1000 °C in the presence of 5 wt % ferrocene and argon carrier gas.[1] TEM imaging of the sample was carried out on a JEOL 3000F. Two-dimensional spectrum images were obtained using an aberration-corrected Nion UltraSTEM 100 dedicated STEM equipped with a Gatan Enfina spectrometer. Carbon materials suffer from beam damage, the dominant mechanism of which is thought to be knock-on, for which there is a threshold energy just above 80 keV.[12] To reduce the beam damage, the UltraSTEM was operated with a beam energy of 60 keV. The energy resolution, measured (at a dispersion of 0.5 eV/pixel) using the full width half-maximum of the zero-loss peak, was 0.5 eV. Thick nanotubes (diameter larger than about 50 nm) were found to produce too much background to be able to distinguish core-loss edges, and so interpretable data could only be obtained from relatively thin (diameter below about 50 nm) nanotubes. The elemental maps shown in Figures 2 and 4 were constructed using the counts contained within the edge for each element. The B and B π^* maps in Figure 4 were reconstructed from data after reducing the noise using a multivariate statistical analysis method described by Lozano-Perez *et al.*[13]

In situ current measurements were carried out using a Nanofactory TEM-STM holder in a JEOL 2010 operated at 200 kV. The B-MWCNTs were mounted on a Au support wire with a second Au wire used for the probe. In order to calculate the resistivity of the nanotubes, the current is assumed to go through the whole cross-section of the nanotube, as there is no hollow core. The length of the nanotube is measured from low-magnification TEM images, but as the experimental setup is viewed in projection and the point of contact between the nanotube and support wire may be difficult to see, the length may be longer than that measured. This means that the resistivity may be overestimated.

Conflict of Interest: The authors declare no competing financial interest.

Acknowledgment. We are grateful to the Engineering and Physical Sciences Research Council (Grant EP/H046550/1; R.J.N., N.G.), (EPSRC Pathways to Impact Awards; N.G.), The Royal Society (N.G.), and the European Research Council (ERC-2009-StG-240500; N.G.) for financial support.

REFERENCES AND NOTES

1. Koós, A.; Dillon, F.; Obraztsova, E. A.; Crossley, A.; Grobert, N. Comparison of Structural Changes in Nitrogen and Boron-Doped Multi-Walled Carbon Nanotubes. *Carbon* **2010**, *48*, 3033–3041.
2. Koós, A.; Nicholls, R. J.; Dillon, F.; Kertész, K.; Biró, L. P.; Crossley, A.; Grobert, N. Tailoring Gas Sensing Properties of Multi-Walled Carbon Nanotubes by *in Situ* Modification with Si, P, and N. *Carbon* **2012**, *50*, 2816–2834.
3. Terrones, M.; Jorio, A.; Endo, M.; Rao, A.; Kim, Y.; Hayashi, T. New Direction in Nanotube Science. *Mater. Today* **2004**, *7*, 30–45.
4. Lee, J. M.; Park, J. S.; Lee, S. H.; Kim, H.; Yoo, S.; Kim, S. O. Selective Electron- or Hole-Transport Enhancement in Bulk-Heterojunction Organic Solar Cells with N- or B-Doped Carbon Nanotubes. *Adv. Mater.* **2011**, *23*, 629–633.
5. Carroll, D. L.; Redlich, P.; Ajayan, P. M.; Curran, S.; Roth, S.; Rühle, M. Spatial Variations in the Electronic Structure of Pure and B-Doped Nanotubes. *Carbon* **1998**, *36*, 753–756.
6. Satishkumar, B. C.; Govindaraj, A.; Harikumar, K. R.; Zhang, J.-P.; Cheetham, A. K.; Rao, C. N. R. Boron-Carbon Nanbotubes from the Pyrolysis of C_2H_2-B_2H_h Mixtures. *Chem. Phys. Lett.* **1999**, *300*, 473–477.
7. Hsu, W. K.; Firth, S.; Redlich, P.; Terrones, H.; Zhu, Y. Q.; Grobert, N.; Schilder, A.; Clark, R. J. H.; Kroto, H. W.; Walton, D. R. M. Boron-Doping Effects in Carbon Nanotubes. *J. Mater. Chem.* **2000**, *10*, 1425–1429.
8. Arenal, R.; de la Peña, F.; Stéphan, O.; Walls, M.; Tencé, M.; Loiseau, A.; Colliex, C. Extending the Analysis of EELS Spectrum-Imaging Data, from Elemental to Bond Mapping in Complex Nanostructures. *Ultramicroscopy* **2008**, *109*, 32–38.
9. Lu, J.; Gao, S.-P.; Yuan, J. ELNES for Boron, Carbon, and Nitrogen K-Edges with Different Chemical Environments in Layered Materials Studied by Density Functional Theory. *Ultramicroscopy* **2012**, *112*, 61–68.
10. Aslam, Z.; Nicholls, R. J.; Koós, A.; Nicolosi, V.; Grobert, N. Investigating the Structural, Electronic and Chemical Evolution of B-Doped Multi-walled Carbon Nanotubes as a Result of Joule Heating. *J. Phys. Chem. C* **2011**, *115*, 25019–25022.
11. Powell, R. L.; Childs, G. E. *American Institute of Physics Handbook*, 3rd ed.; McGraw-Hill: New York, 1972.
12. Smith, B. W.; Luzzi, D. E. Electron Irradiation Effects in Single Wall Carbon Nanotubes. *J. Appl. Phys.* **2001**, *90*, 3509–3515.
13. Lozano-Perez, S; de Castro Bernal, V; Nicholls, R. J. Achieving Sub-Nanometre Particle Mapping with Energy-Filtered TEM. *Ultramicroscopy* **2009**, *109*, 1217–1228.